


Efimovian three-body potential from broad to narrow Feshbach resonancesJ. van de Kraats^{1,*}, D. J. M. Ahmed-Braun¹, J.-L. Li^{1,2} and S. J. J. M. F. Kokkelmans¹¹*Eindhoven University of Technology, P.O. Box 513, 5600 MB Eindhoven, The Netherlands*²*Institut für Quantenmaterie and Center for Integrated Quantum Science and Technology IQ ST, Universität Ulm, D-89069 Ulm, Germany* (Received 25 October 2022; accepted 20 January 2023; published 1 February 2023; corrected 14 February 2023)

We analyze the change in the hyperradial Efimovian three-body potential as the two-body interaction is tuned from the broad to narrow Feshbach resonance regime. Here, it is known from both theory and experiment that the three-body dissociation scattering length a_- shifts away from the universal value of $-9.7 r_{\text{vdW}}$, with $r_{\text{vdW}} = \frac{1}{2}(mC_6/\hbar^2)^{1/4}$ the two-body van der Waals range. We model the three-body system using a separable two-body interaction that takes into account the full zero-energy behavior of the multichannel wave function. We find that the short-range repulsive barrier in the three-body potential characteristic for single-channel models remains universal for narrow resonances, while the change in the three-body parameter originates from a strong decrease in the potential depth. From an analysis of the underlying spin structure we further attribute this behavior to the dominance of the two-body interaction in the resonant channel compared to other nonresonant interactions.

DOI: [10.1103/PhysRevA.107.023301](https://doi.org/10.1103/PhysRevA.107.023301)**I. INTRODUCTION**

In his seminal papers [1,2], Efimov predicted the appearance of an infinite and geometrically spaced set of three-particle bound states as the pairwise interaction becomes resonant. These Efimov states are bound by a universal attractive potential, decaying asymptotically as $-1/R^2$ for three particles at root mean square separation R . In trapped ultracold atomic gases the Efimov effect induces log-periodic peaks in the atom loss rate, driven by enhanced three-body recombination when an Efimov trimer crosses into the three-particle continuum [3–6]. The position of the loss peak associated with the ground Efimov state sets a characteristic length scale a_- , commonly referred to as the three-body parameter. In three-body systems with zero-range interactions, introducing a three-body parameter is necessary to regularize the scale-invariant unbounded Efimov spectrum [5].

Despite its short-range nature, experiment has revealed that the three-body parameter in different atomic species attains a value close to $a_- = -9.7 r_{\text{vdW}}$ [7–11], where $r_{\text{vdW}} = \frac{1}{2}(mC_6/\hbar^2)^{1/4}$ is the van der Waals length associated with the long-range two-body interaction. Subsequent theoretical studies found that this “van der Waals universality” originates from a characteristic suppression of the two-body wave function when $r < r_{\text{vdW}}$, where r is the two-particle separation [12,13]. This suppression leads to the appearance of a strong repulsive barrier in the three-body potential at mean square separations $R \approx 2 r_{\text{vdW}}$, which shields the particles from probing the nonuniversal short-range detail of the atomic species.

The above-mentioned theoretical analyses are based on single-channel interaction potentials, which are expected to be accurate provided that the intrinsic length scale r_* due

to the resonance width is much smaller than the potential range. This broad resonance regime may be defined by a large resonance strength parameter $s_{\text{res}} = \bar{a}/r_* \gg 1$ [14], where $\bar{a} \approx 0.955978 r_{\text{vdW}}$ is the mean scattering length of the van der Waals interaction [15]. The opposite case of a narrow resonance, where $s_{\text{res}} \ll 1$, is characterized by universal behavior in terms of the dominant length scale $r_* \gg r_{\text{vdW}}$. In this limit, treatments of the three-body problem which neglect the details of the van der Waals interaction found the three-body parameter to be determined universally as $a_- = -10.9 r_*$ [6,16–18]. Connecting the broad and narrow resonance limits through the intermediate regime where $s_{\text{res}} \approx 1$ with a van der Waals interaction model remains to be desired, in particular, given that recent experiments in this regime in ^{39}K revealed clear deviations from both universal limits [11]. A key aspect of this problem is the change in structure of the trimer and its associated potential energy surface as a function of the resonance strength, which will be the central topic of this paper.

In this work we study the Efimovian three-body potential using a realistic multichannel two-body van der Waals interaction, which can be easily tuned to probe a wide regime of resonance strengths. To solve the three-body problem we approximate this interaction by a separable potential which reproduces the zero-energy wave function of the original interaction. We then derive an effective three-body potential from the open-channel three-body wave function, which models the actual three-body potential that binds the Efimov state. Subsequently, we study the dependence of this potential on the resonance strength s_{res} and provide an analysis of our findings in terms of the multichannel structure underlying the three-body dynamics.

This paper will be structured as follows. In Sec. II we outline our approach at the two-body level, first defining a two-channel model interaction with a Feshbach resonance that

*j.v.d.kraats@tue.nl

can be tuned from the broad to narrow resonance strength limit. Subsequently, we formulate a separable approximation to this interaction. In Sec. III we move to the three-body level, which we analyze first in momentum space to facilitate our actual computations and then subsequently in position space for our analysis of the three-body potential. In Sec. IV we present and analyze our results, after which we conclude this paper in Sec. V.

II. TWO-BODY INTERACTION MODELS

A. Model two-channel interaction

In this section we develop a flexible two-channel model that can be tuned to produce a Feshbach resonance with a given Breit-Wigner shape [19–21]. We label the two scattering channels $\sigma = \{1, 2\}$, with internal energies ε_σ and define the two-body Hamiltonian operator

$$H = H^0 + V = \begin{pmatrix} H_1^0 + V_{1,1} & V_{1,2} \\ V_{2,1} & H_2^0 + V_{2,2} \end{pmatrix}, \quad (1)$$

where H^0 contains the internal and kinetic energies of the particles and V the pairwise interactions. Expressed in the interparticle distance r , the diagonal interactions are of van der Waals type [22,23]

$$V_{1,1}(r) = V_{2,2}(r) = C_6 \left(\frac{r_0^4}{r^{10}} - \frac{1}{r^6} \right), \quad (2)$$

with C_6 the species-specific dispersion coefficient. The parameter r_0 controlling the short-range barrier is tuned such that both channels have eight uncoupled dimer states, which we confirm is sufficiently deep such that the scattering is universally determined by the van der Waals tail. The off-diagonal terms of the interaction represent spin-exchange processes, which we model using a Gaussian form inspired by Ref. [21]

$$V_{1,2}(r) = V_{2,1}(r) = \beta e^{-\alpha(r-r_W)^2}, \quad (3)$$

where $\{\beta, \alpha, r_W\}$ are tuneable parameters. To enforce the short-range nature of the spin-exchange interaction, we fix $r_W = 0.15 r_{\text{vdW}}$ [24]. We will take the channel $\sigma = 1$ to be energetically open and set its internal energy as $\varepsilon_1 = 0$ such that $H_1^0(r) = -\hbar^2 \nabla_r^2 / m$. The channel $\sigma = 2$, referred to as the closed channel, has a magnetic-field-dependent internal energy $H_2^0(r, B) = -\hbar^2 \nabla_r^2 / m + \varepsilon_2(B)$. To model the Feshbach resonance, we define [19]

$$\varepsilon_2(B) = \varepsilon_b + \delta\mu(B - B_{\text{res}}), \quad (4)$$

where ε_b is the bare binding energy of the resonant bound state in the closed channel, $\delta\mu$ the differential magnetic moment of the particles which is inferred from experiment, and B_{res} the bare resonant magnetic field. Given a background scattering length a_{bg} , resonance width ΔB , and resonant magnetic field B_0 , we can extract an associated set of model parameters $\{r_0, \alpha, \beta, r_W, B_{\text{res}}\}$. The details of this mapping are outlined in Appendix A. The resulting resonance strength is obtained as [14]

$$s_{\text{res}} = \frac{m}{\hbar^2} \bar{a} a_{\text{bg}} \delta\mu \Delta B, \quad (5)$$

which quantifies the ratio r_*/\bar{a} as mentioned in Sec. I.

B. EST separable potential

As pointed out in previous studies, the universal van der Waals three-body parameter and three-body potential can be reproduced by accounting for the full finite-range detail of the van der Waals interaction [12]. Similarly, it was recently shown that reproducing the three-body recombination rate for resonances of intermediate strength in ^{39}K requires an inclusion of the exact three-body spin structure in the Hamiltonian [25]. Such approaches, however, are complicated numerically and not conducive to our goal of developing a simple and flexible model. Fortunately, it was pointed out in Refs. [13,26] that van der Waals universality can be reproduced using a much simpler model, based on the Ernst, Shakin, and Thaler (EST) separable potential [27]. In this section we develop such an approach for our multichannel interaction. The crucial point is that we approximate the interaction in such a way that the full two-body wave function at zero energy is taken into account, while retaining the simplicity of a single-term separable potential.

For an arbitrary multichannel interaction V , we may define a separable approximation as $V^{\text{sep}} = |g\rangle \xi \langle g|$. In the EST formalism, the form factor $|g\rangle$ and potential strength ξ are derived from a given eigenfunction $|\psi\rangle$ of the full multichannel Hamiltonian

$$|g\rangle = V |\psi\rangle, \quad \xi^{-1} = \langle \psi | V | \psi \rangle. \quad (6)$$

With these definitions we may show that $|\psi\rangle$ is also an eigenfunction of the Hamiltonian where V is replaced with V^{sep} with the exact same eigenvalue [27]. Adopting the approach of the authors of Ref. [13], we take $|\psi\rangle$ to be the zero-energy scattering state, such that our model takes as input the low-energy scattering detail of the actual interaction. The separable interaction has an associated separable t matrix, given by the Lipmann-Schwinger equation [28]

$$t^{\text{sep}}(z) = V^{\text{sep}} + V^{\text{sep}} G_0(z) t^{\text{sep}}(z). \quad (7)$$

Here $G_0(z) = (z - H_0)^{-1}$ is the Green's function in the absence of interactions. We define its s -wave eigenstates as $|k, \sigma\rangle$, where $k = |\mathbf{k}|$ is the relative momentum and σ the scattering channel introduced in the previous section. In this basis, the transition matrix may be written as

$$t_{\sigma', \sigma}^{\text{sep}}(z, k', k) = g_{\sigma'}(k') \tau(z) g_{\sigma}^*(k), \quad (8)$$

where $t_{\sigma', \sigma}^{\text{sep}}(z, k', k) = \langle k', \sigma' | t^{\text{sep}}(z) | k, \sigma \rangle$ and $g_{\sigma}(k) = \langle k, \sigma | g \rangle$. Explicit expressions for $\tau(z)$ and $g_{\sigma}(k)$ are given in Appendix B. To obtain the eigenfunction $|\psi\rangle$ we explicitly diagonalize the two-body Hamiltonian, using a mapped grid discrete variable representation [29,30]. For the broad resonance limit $s_{\text{res}} \gg 1$, the Feshbach resonance is well approximated by a potential resonance in a single-channel model with the interaction in Eq. (2). In this case, we obtain $|\psi\rangle$ using an efficient Numerov method [31]. The behavior of the form factor as a function of resonance width is illustrated in Fig. 1. Note that the arbitrary normalization of the form factors is fixed by taking $g_1(0) = 1$. Since the open-channel component of the wave function is independent of s_{res} (see

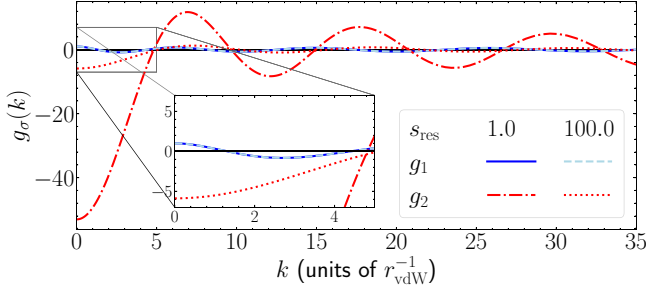


FIG. 1. The form factors $g_\sigma(k)$ as a function of momentum k , tuned to two different resonance strengths. Inset shows a zoom of the low momentum regime, where one observes the normalization $g_1(0) = 1$.

Sec. IV B), the open-channel form factors are much less sensitive to changes in the resonance strength than the closed-channel form factors.

We emphasize that the EST model is based on the zero-energy wave function and hence loses accuracy when used to describe deep bound states. To illustrate this behavior we computed the shallow dimer energy around the eighth potential resonance in the two-channel model, both by a direct numerical solution of the multichannel Schrödinger equation and via the EST potential of this section. In the later case, a dimer solution is found through the condition $\tau^{-1}(\varepsilon) = 0$, with $\varepsilon < 0$ the binding energy. The two results are compared in Fig. 2, where we observe that the EST potential is most accurate near threshold and is thus naturally suited to treat states near resonance. For smaller scattering lengths the EST potential becomes inaccurate for broad resonances where the dimer becomes too strongly bound, but remains reasonably accurate in describing narrower resonances. In this paper we only concern ourselves with the near-resonant regime $a \gg r_{\text{vdW}}$, where the EST potential is accurate regardless of the resonance strength.

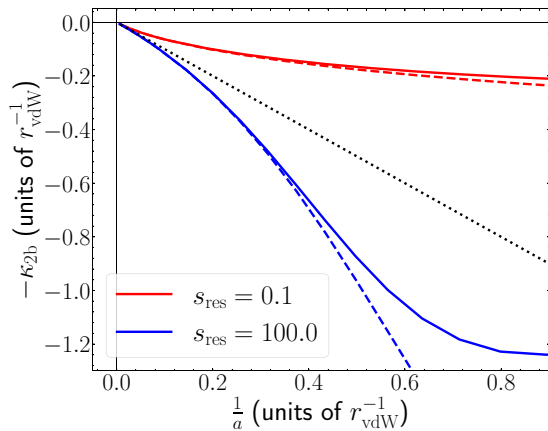


FIG. 2. Binding wave number $\kappa_{2b} = \sqrt{m|\varepsilon|/\hbar^2}$ of the Feshbach dimer that manifests in the two-channel model of Sec. II A, as a function of inverse scattering length. Results are shown both with the EST model potential (solid lines) and a direct solution of the multichannel Schrödinger equation (dashed lines). We show results for two different resonance strengths and additionally plot the universal resonant result $\kappa_{2b} \sim 1/a$ as the black dotted line.

III. THREE-BODY APPROACH

A. Three-body integral equation

To find the three-body bound-state energy E and wave function $|\Psi\rangle$, we adopt the methodology of the authors of Ref. [18]. Three-body states are expressed in the s -wave basis $|k, p, \sigma, \sigma_3\rangle$. Here $\{k, p\}$ are the dimer and atom-dimer Jacobi momenta, respectively, $\sigma = \sigma_1\sigma_2$ gives the channel of the two-body system as introduced in Sec. II, where the underline denotes symmetrization, and σ_3 the spin of the third particle (in general in this section we shall use subscripts to label particles 1, 2, and 3). The internal energy of the three particles as dictated by the spin states will be denoted as $E(\sigma, \sigma_3)$. The wave function $|\Psi\rangle$ is written into the Faddeev decomposition [32,33]

$$|\Psi\rangle = (1 + P_+ + P_-)|\bar{\Psi}\rangle, \quad (9)$$

with $|\bar{\Psi}\rangle$ the Faddeev component and P_\pm cyclic permutation operators of the particle indices. For the EST separable two-body transition matrix [see Eq. (8)], the state $|\bar{\Psi}\rangle$ projected on our three-body basis can be formulated as

$$\langle k, p, \sigma, \sigma_3 | \bar{\Psi} \rangle = \frac{g_\sigma(k)F_{\sigma_3}(p)}{E - \frac{\hbar^2 k^2}{m} - \frac{3}{4} \frac{\hbar^2 p^2}{m} - E(\sigma, \sigma_3)}. \quad (10)$$

Here the function $F_{\sigma_3}(p)$ captures the dynamics of the third particle and is obtained from the one-dimensional integral equation,

$$\tau^{-1}[Z_{\sigma_3}(p)]F_{\sigma_3}(p) = \sum_{\sigma'_3} \int d^3\mathbf{q} \mathcal{Z}_{\sigma_3\sigma'_3}(\mathbf{p}, \mathbf{q})F_{\sigma'_3}(q), \quad (11)$$

known as the Skorniakov-Ter-Martirosian (STM) equation. Here $Z_{\sigma_3}(\kappa, p) = E - 3\hbar^2 p^2/(4m) - E_{\sigma_3}$, with E_{σ_3} the internal energy of the third particle and the kernel $\mathcal{Z}_{\sigma_3\sigma'_3}(\mathbf{p}, \mathbf{q})$ is given as

$$\begin{aligned} \mathcal{Z}_{\sigma_3\sigma'_3}(\mathbf{p}, \mathbf{q}) = & \sum_{\sigma\sigma'} \frac{g_\sigma(|\mathbf{q} + \frac{1}{2}\mathbf{p}|)g_{\sigma'}^*(|\frac{1}{2}\mathbf{q} + \mathbf{p}|)}{E - \frac{\hbar^2}{m}(p^2 + q^2 + \hat{\mathbf{p}} \cdot \hat{\mathbf{q}}) - E(\sigma', \sigma'_3)} \\ & \times \langle \sigma, \sigma_3 | 2P_+^s | \sigma', \sigma'_3 \rangle. \end{aligned} \quad (12)$$

Here P_+^s is the cyclic permutation operator that acts solely in the space of internal states and the factor of 2 accounts for the anticyclic permutation. We will label distinct single-particle states in alphabetical order, taking the open two-body channel as $|\sigma = 1\rangle \equiv |aa\rangle$ and the closed-channel as $|\sigma = 2\rangle \equiv |bc\rangle$. The presence of P_+^s in the integral equation expresses that the three-body problem is complicated by the appearance of the additional nonresonant closed channels $|ab, c\rangle$ and $|ac, b\rangle$. However, the nonresonant interaction in $|ab\rangle$ and $|ac\rangle$ is much weaker than the resonance enhanced interaction in $|bc\rangle$, which we illustrate numerically in Appendix C. Hence, we choose to neglect $V_{ab,ab}$ and $V_{ac,ac}$, which restricts the multichannel three-body equation (11) to the channels $|aa, a\rangle$ and $|bc, a\rangle$. This is equivalent to the fixed spectating spin approximation, which is widely implemented in previous studies of the three-body problem [11,16,25,34–38].

As was shown in Ref. [18], the open-channel projection $\langle k, p, aa, a | \bar{\Psi} \rangle$ of the Faddeev component completely decouples from the closed channel $|bc, a\rangle$. Since $\langle k, p, aa, a | \bar{\Psi} \rangle$

contains the long-range physics associated with the Efimov effect, we only need to solve an effective single channel (ESC) form of Eq. (11), which contains purely the open-channel component of the two-body transition matrix. Effects of the closed-channel are then included purely at the two-body level. Note that the situation is entirely different for closed channels of the type $|ab\rangle$, where one particle conserves its spin [18]. We choose to exclude this special case from our model, but will comment on it briefly in Sec. IV C. For closed channels of the type $|bb\rangle$ our model applies without any complications.

B. Effective three-body potential

The momentum space approach as outlined in the previous section will be used to solve the three-body problem. However, for the analysis of the Efimovian three-body potential, we need to make a transformation to position space. In this section we give a brief overview of the hyperspherical formalism in which the Efimovian potential is usually expressed. For a more detailed discussion we refer to Refs. [5,39–41].

For identical particles, the Jacobi dimer separation r_i and atom-dimer separation ρ_i are transformed to a hyperradius R and hyperangle α_i ,

$$\tan \alpha_i = \frac{\sqrt{3}r_i}{2\rho_i}, \quad R^2 = r_i^2 + \frac{4}{3}\rho_i^2. \quad (13)$$

Here $i = 1, 2, 3$ denotes the Jacobi index, which we will suppress in this section. As the notation implies, R is invariant to a change in Jacobi set. The hyperangle α is often denoted together with the polar and azimuthal angles of the unit vectors $\hat{\mathbf{r}}$ and $\hat{\boldsymbol{\rho}}$ as $\boldsymbol{\Omega}$. We expand the open-channel wave function into a complete and orthonormal set of hyperangular functions $\Phi_\nu(R, \boldsymbol{\Omega})$, by the following expansion:

$$\langle R, \boldsymbol{\Omega}, \underline{aa}, a | \Psi \rangle = \frac{1}{R^{\frac{5}{2}}} \sum_{\nu=0}^{\infty} f_\nu(R) \Phi_\nu(R, \boldsymbol{\Omega}). \quad (14)$$

Note that we will suppress spin indices for this expansion as we will always use the open-channel component of the three-body wave function. The hyperangular functions $\Phi_\nu(R, \boldsymbol{\Omega})$ are eigenfunctions of the angular momentum part of the three-body Schrödinger equation. The index ν is usually referred to as the hyperspherical channel and the associated expansion coefficient $f_\nu(R)$ as the hyperradial wave function. It obeys the following set of coupled equations [42]:

$$\left[-\frac{d^2}{dR^2} + \frac{\lambda_\nu(R) - \frac{1}{4}}{R^2} + \kappa^2 + Q_{\nu\nu}(R) \right] f_\nu(R) + \sum_{\nu' \neq \nu} \left[Q_{\nu\nu'}(R) + 2P_{\nu\nu'}(R) \frac{d}{dR} \right] f_{\nu'}(R) = 0. \quad (15)$$

Here $\lambda_\nu(R)$ is the eigenvalue associated with the hyperangular function $\Phi_\nu(R, \boldsymbol{\Omega})$, where R is interpreted as a parameter of the eigenvalue equation. We also introduced a trimer binding wave number $\kappa = \sqrt{m|E|/\hbar^2}$, which we use going forward. Equation (15) defines an infinite set of equations coupled

through the presence of the coupling potentials

$$P_{\nu\nu'}(R) = -\left\langle \Phi_\nu \left| \frac{\partial}{\partial R} \right| \Phi_{\nu'} \right\rangle_{\boldsymbol{\Omega}}, \quad \text{and} \quad (16)$$

$$Q_{\nu\nu'}(R) = -\left\langle \Phi_\nu \left| \frac{\partial^2}{\partial R^2} \right| \Phi_{\nu'} \right\rangle_{\boldsymbol{\Omega}}.$$

The inner products on the right-hand side should be taken over the space of angular coordinates $\boldsymbol{\Omega}$. The coupling potentials quantify the dependence of the hyperangular distribution on the hyperradius and are often referred to as nonadiabatic contributions to the three-body problem [42]. In the so-called scale-free region, where $r_{\text{vdW}} \ll R \ll |a|$, one may show that the eigenvalue λ becomes independent of the hyperradius [5]. This has the consequence that all nonadiabatic contributions vanish and the coupled set presented in Eq. (15) uncouples into single-particle Schrödinger equations with “effective” hyperradial three-body potentials $U_m(R) = (\lambda_\nu - \frac{1}{4})/R^2$. The Efimov channel $\nu = 0$ has eigenvalue $\lambda_0 = -s_0^2$, with $s_0 \approx 1.00624$. Thus the associated three-body potential is attractive, inducing the Efimov effect with its characteristic $1/R^2$ scaling. In the scale-free region all channels with $\nu \neq 0$ have associated three-body potentials that are purely repulsive [42].

Due to the nontrivial behavior of the coupling potentials in the short-range regime, the full behavior of the effective potential is very complicated. Upon solving the STM equation (11), however, we can use the three-body wave function to derive an approximation to the Efimovian three-body potential in the scale-free region. First, we formulate the three-body probability as

$$\bar{P}_{\boldsymbol{\Omega}}(R) \sim R^5 \int_0^{\frac{\pi}{2}} d\alpha \sin^2(2\alpha) \int_{-1}^1 dx |\Psi(R, \alpha, x)|^2, \quad (17)$$

where $x = \hat{\mathbf{r}} \cdot \hat{\boldsymbol{\rho}}$ gives the inner product of the two Jacobi vectors and $\Psi(R, \alpha, x)$ is obtained by a Fourier transformation of Eq. (9). By virtue of the orthonormality of the hyperangular functions $\Phi(R, \boldsymbol{\Omega})$ it is possible to use the three-body probability to derive an effective three-body potential, a method also applied in Ref. [13]. The validity of this method relies on the efficiency of the hyperspherical expansion in Eq. (14). Since the Efimov channel is the only attractive channel, we are justified in neglecting all higher-lying repulsive channels which suppress the local probability [12]. Then the expansion contains only one term and the resulting three-body probability is equal to $|f_0(R)|^2$. Since we can choose $f_0(R)$ to be real by the normalization of the wave function, the following expression for an effective three-body potential follows from Eq. (15):

$$U_{\text{eff}}(R) = \frac{1}{\sqrt{\bar{P}_{\boldsymbol{\Omega}}(R)}} \frac{d^2}{dR^2} \sqrt{\bar{P}_{\boldsymbol{\Omega}}(R)} - \kappa^2. \quad (18)$$

At unitarity this effective potential is expected to be a good approximation of the actual Efimov potential in the scale-free region. In particular, it is sufficiently accurate to reproduce the characteristic repulsive barrier around $R \approx 2 r_{\text{vdW}}$ and the potential well which appear for broad resonances, as was shown in Ref. [13].

TABLE I. Parameters of the physical resonances used as a starting point for our computations. The value of s_{res} in the last column will be varied with all other parameters held fixed. Data taken from (^{39}K : [43]), (^{85}Rb : [44,45]), and (^{133}Cs : [14,46]).

Species	B_0 [G]	a_{bg} [r_{vdW}]	$\delta\mu$ [E_{vdW}/G]	s_{res}
^{39}K	33.50	-0.31	-0.154	2.46
^{85}Rb	155.04	-5.40	-0.517	28.6
^{133}Cs	-11.7	17.02	1.21	565
^{133}Cs	547.0	24.74	0.94	167

IV. RESULTS

To fix the degrees of freedom in the model of Sec. II A we take sets of resonance parameters measured from physical resonances, summarized in Table I. We then shift the resonance strength s_{res} away from the physical value by altering ΔB , keeping all other parameters fixed. As reported in Ref. [37], the change in the three-body parameter with varying resonance strength becomes more abrupt as a_{bg} approaches the value of a_- in the open-channel potential. We check whether our model reproduces this behavior by artificially altering the rubidium resonance in Table I such that $a_{\text{bg}} = -9.75 r_{\text{vdW}}$, noting that the open-channel potential has a three-body parameter $a_- = -10.85 r_{\text{vdW}}$ in the EST approximation.

A. Efimov spectra

We first apply our model to the computation of the Efimov spectra and associated three-body parameters as a function of the Feshbach resonance strength. First, we show in Fig. 3 the spectrum of the two lowest-lying Efimov states for finite scattering lengths surrounding the Feshbach resonance.

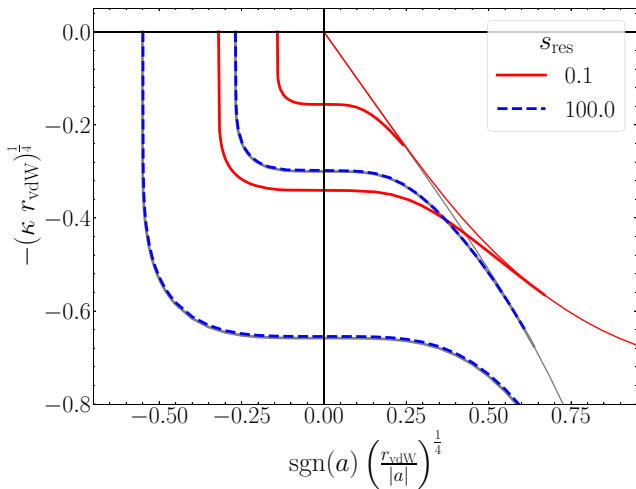


FIG. 3. Binding wave number of the two lowest-lying Efimov states as a function of the inverse scattering length, computed at two different resonance strengths. For $a > 0$ the atom-dimer thresholds from Fig. 2 are plotted with thin lines. Gray lines show the energies obtained from a single-channel EST model, which corresponds with the broad-resonance limit $s_{\text{res}} \rightarrow \infty$. Multichannel model used to produce this figure is tuned to the ^{39}K resonance in Table I.

Comparing with the broad resonance limit $s_{\text{res}} \rightarrow \infty$, we find that, as the resonance strength is decreased, the Efimov spectrum is squeezed into a smaller area of the $(\kappa, 1/a)$ plane, corresponding to an increase of the three-body parameter $|a_-|$. Alternatively, we can also define the three-body parameter via the wave number κ_* of the ground-state trimer at resonance, which decreases as the resonance becomes narrow.

The shift in three-body parameters can be more clearly seen in Fig. 4, where we show a scan of $|a_-|$ and κ_* from the broad to narrow resonance limit. For the sake of comparison, Fig. 4 also contains experimental data for a select set of physical resonances. As the resonance strength decreases, the three-body parameter $|a_-|$ shows a monotonous increase, consistent with findings in earlier studies such as Refs. [36,37]. Within the narrow resonance limit our results approach the universal limit $a_- = -10.9 r_*$. The effect of the background scattering length can mainly be observed in the intermediate strength regime, where larger negative values of a_{bg} tend to push the three-body parameter closer to the universal broad resonance value for a larger portion of the resonance strength regime. This finding is consistent with more artificial models of the two-body interaction, such as the approach adopted in Ref. [37]. However, our more realistic EST model strongly suppresses the sensitivity of the three-body parameter to the background scattering length. Similarly, we find that replacing our EST potential by a simple ultraviolet cutoff greatly increases the sensitivity to a_{bg} . This is especially true for the binding wave number κ_* , whose dependence on a_{bg} is negligible on the scale of Fig. 4. In Ref. [37], the sensitivity of κ_* to a_{bg} was attributed to beyond effective range effects. For van der Waals potentials, the effective range r_e^{vdW} as a function of s_{res} is known to behave as [47,48]

$$r_e^{\text{vdW}} = \frac{\bar{a}}{6} \left(\frac{\Gamma(\frac{1}{4})}{\Gamma(\frac{3}{4})} \right)^2 \left[1 - 2\frac{\bar{a}}{a} + 2\left(\frac{\bar{a}}{a}\right)^2 \right] - \frac{\bar{a}}{s_{\text{res}}} \left[1 - \frac{a_{\text{bg}}}{a} \right]^2. \quad (19)$$

The first term contains all nonresonant contributions that give a universally determined effective range at unitarity [49], while the second term captures the additional contribution due to the Feshbach resonance. Since the EST model reproduces the zero-energy wave function exactly, the effective range in our multichannel model is well described by this equation. At resonance, where $a_{\text{bg}}/a \rightarrow 0$, the effective range becomes fully independent of the background scattering length similar to the three-body parameter κ_* .

B. Three-body repulsion

Having confirmed that the three-body parameter in our model scales as expected in both the narrow and broad resonance limits, we now move on to a position space analysis using the formalism of Sec. III B. Given that our results are largely insensitive to a_{bg} at the position of the resonance, we limit ourselves in this section to the ^{39}K resonance with $a_{\text{bg}} = -0.31 r_{\text{vdW}}$. Before analyzing the three-body state directly, it is instructive to consider the two-body scattering wave function $\langle r|\psi\rangle$ [see Eq. (B2)] that is used to construct the EST potential. To this end we plot the open and closed channel radial components of the wave function for a set of

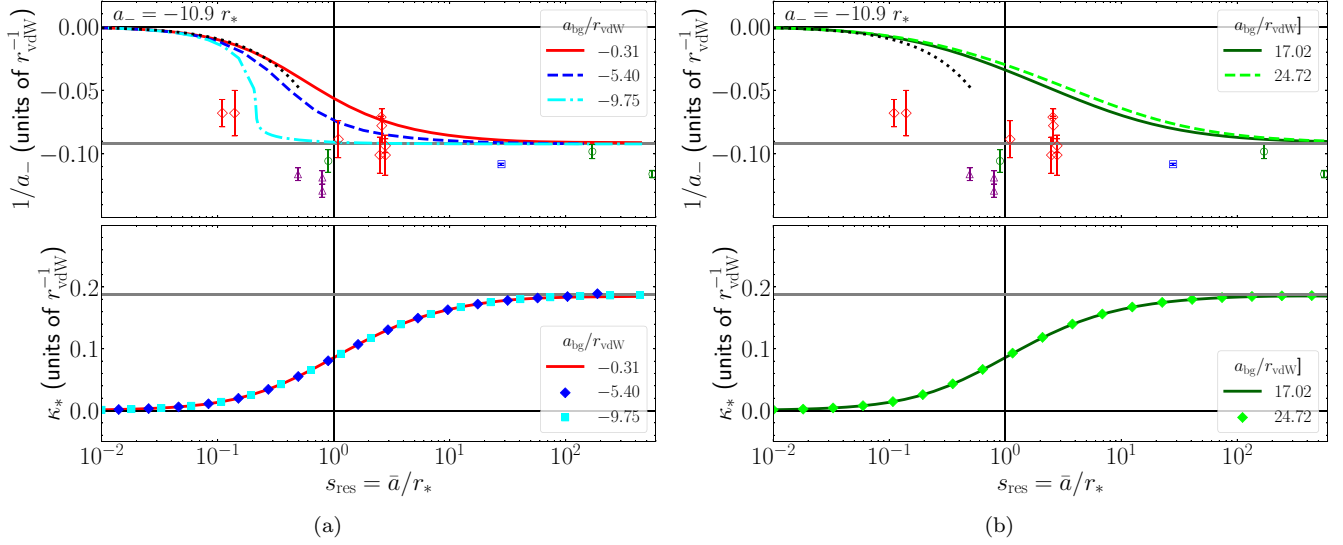


FIG. 4. Plots of the three-body parameters as a function of resonance strength for (a) negative a_{bg} and (b) positive a_{bg} . In the top panels we show the inverse of the dissociation scattering length a_- associated with the ground-state Efimov trimer. Here colored lines show the results of our multichannel model for different background scattering lengths. Scatter points represent experimental data, measured in ^{133}Cs (green circles) [7], ^7Li (purple triangles) [8,9], ^{85}Rb (blue squares) [10], and ^{39}K (red diamonds) [11,50]. The color of the line plots is chosen to match the data points, e.g., the red plots were computed using resonance parameters matching a resonance in ^{39}K . In the narrow resonance limit $s_{res} \ll 1$ we illustrate the limiting behavior $a_- = -10.9 r_*$ as a black dotted line. In the bottom panels we plot the trimer binding wave number κ_* at resonance. Here results for different background scattering length practically overlap on the scale shown, so we use scatter plots to distinguish between them. In both the upper and lower panels the three-body parameter obtained with a single-channel EST model, corresponding with the broad resonance limit $s_{res} \gg 1$, is shown as a gray horizontal line.

different resonance strengths in Fig. 5, normalized such that the wave function asymptotes to 1 for $r \gg r_{vdW}$. As predicted by multichannel resonance theory the open-channel amplitude $|u_1(r)|$ is independent of s_{res} , while the closed-channel amplitude $|u_2(r)|$ scales as $\sim 1/\sqrt{s_{res}}$ [51]. Previous analyses of single-channel van der Waals interactions connected the suppression of the two-body wave function below distances of

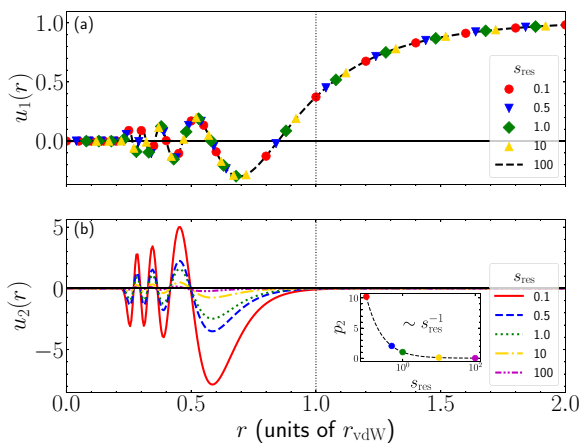


FIG. 5. (a) Open and (b) closed channel functions $u_1(r)$ and $u_2(r)$ for different values of the resonance strength, computed at unitarity for the Feshbach resonance with $a_{bg} = -0.31 r_{vdW}$. The $r = r_{vdW}$ boundary is emphasized by the black dotted line. The normalization is chosen such that the total wave function asymptotes to unity in the long range. The inset in (b) shows the scaling of the integrated closed-channel two-body probability $p_2 = \int dr |u_2(r)|^2$ with s_{res} .

$1 r_{vdW}$ to the appearance of a universal repulsive barrier in the three-body potential at $R \approx 2 r_{vdW}$ [12,13]. In the two-channel case this suppression persists in the open-channel component, while there appears an increase in total short-range two-body probability due to the finite lifetime of the closed-channel state.

To examine the effect of the closed-channel on the three-body level we first compute the three-body probability in the $\{R, \alpha\}$ plane by omitting the integration over the hyperangle in Eq. (17). The results are shown in Fig. 6. Here the effect of the open-channel suppression is highlighted by plotting the boundary beyond which any two particles approach below the van der Waals length. As expected, the three-body probability is strongly suppressed beyond this boundary for the broad resonance (the first two panels of Fig. 6), where the closed-channel component is small. Interestingly, as we tune our interaction towards the narrow resonance regime and the closed-channel amplitude increases we see no additional penetration of the region of open-channel suppression. Instead, we find that both the average and the spread of the three-body wave function in the hyperradial coordinate increase. This suggests that the open-channel suppression of two-body probability remains a dominant factor for small hyperradii, strongly suppressing the three-body probability regardless of resonance strength. The increase in closed-channel two-body amplitude mainly impacts the intermediate to long-distance regime where $R > 2 r_{vdW}$. As was noted before [12,13], the appearance of a three-body repulsive barrier is associated with a repulsive potential energy peak due to the nonadiabatic correction $Q_{00}(R)$ in Eq. (15), reminiscent of an angular momentum barrier. This peak arises due to a squeezing of the

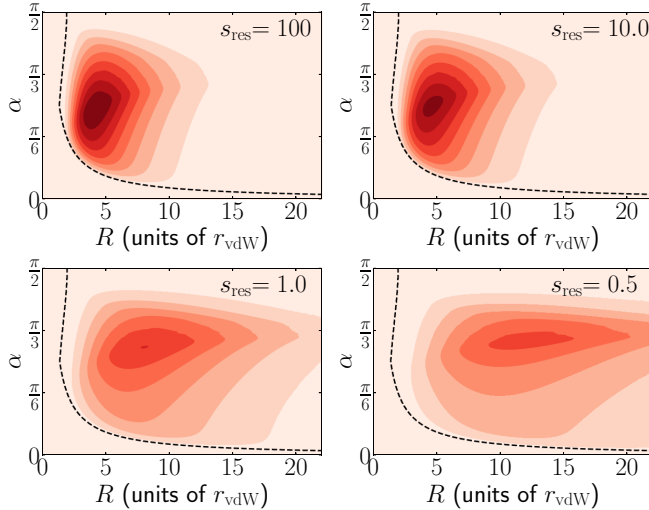


FIG. 6. Contour plots of the three-body probability at four different values of s_{res} . Computed using the ^{39}K resonance with $a_{\text{bg}} = -0.31 r_{\text{vdW}}$ as input. The boundary below which any two particles approach closer than $1 r_{\text{vdW}}$ is shown by a black dashed line. Format inspired by Ref. [13].

hyperangular distribution function $\Phi(R, \Omega)$ as R decreases, driven by the short-range two-body suppression. Our results in Fig. 6 show that the location of this barrier remains universally determined by the van der Waals length also near a narrow resonance.

We now proceed by integrating out the hyperangle to obtain $\bar{P}_{\Omega}(R)$ and use Eq. (18) to derive the effective three-body potential. The results are plotted in Fig. 7, where, for the sake of comparison, we also show the result with a single-channel interaction (corresponding with $s_{\text{res}} \rightarrow \infty$) and the universal $\sim 1/R^2$ potential from zero-range theory which corresponds with the limit $R/r_{\text{vdW}} \rightarrow \infty$ [5]. Consistent with Fig. 6, a decreasing resonance strength manifests most strongly in the intermediate to long distance regime, where we observe a strong decrease in the depth of the effective potential that pushes the Efimov state closer to threshold. This corresponds with a decrease of the binding energy κ_* , as observed in Fig. 4. To verify whether this behavior continues into the narrow resonance limit, we tracked the effective potential up to $s_{\text{res}} = 0.01$. Here the potential at larger separations becomes practically flat, signifying that all hyperradii have approximately equal probability. To obtain a more quantitative characterization of the decrease in depth we plot the minimum of the effective potential as a function of s_{res} , shown in the inset of Fig. 7. In the broad resonance limit we find that the depth of the barrier scales with $1/\sqrt{s_{\text{res}}}$, and is hence inversely proportional to the closed-channel amplitude as plotted in Fig. 5. Consistent with Fig. 6 the position of the repulsive barrier is set by the van der Waals length with the relation $R \approx 2 r_{\text{vdW}}$, regardless of the resonance strength.

To supplement our findings we also computed three-body effective potentials for particles interacting via exponentially decaying potentials, common in nuclear physics. Here the three-body parameter was predicted to be likewise different compared to the single-channel van der Waals interaction

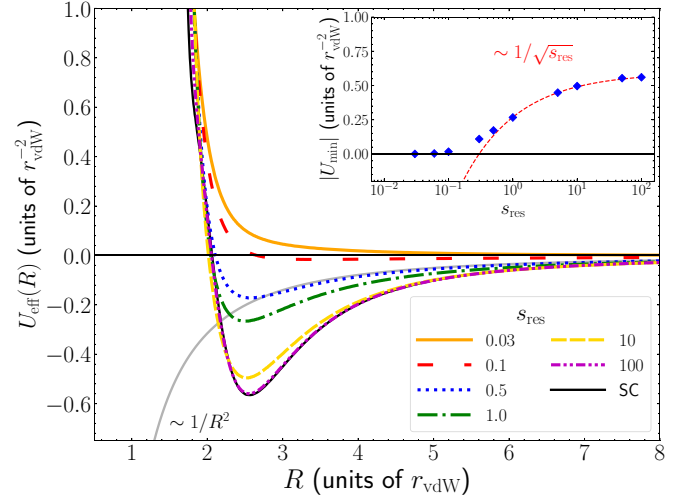


FIG. 7. Plot of the effective three-body potential as a function of the hyperradius, computed with starting parameters taken from the ^{39}K resonance as outlined in Table I. Colored lines show the effective potential at different values of the resonance strength parameter. In the regime of small hyperradius $R \lesssim r_{\text{vdW}}$ there appear unphysical and meaningless oscillations in the potential as artifacts of the model [13], which we removed from the plot to avoid unnecessary clutter. Black line shows the effective potential computed by using the associated single-channel EST model. Gray line shows the asymptotic $\sim 1/R^2$ Efimov attraction as follows from the zero-range theory. Plot includes an inset showing the scaling of the minimum $U_{\text{min}}(R)$ of the effective potential with s_{res} .

[26]. However, in contrast to the multichannel case, we find that this change originates from a shift in the location of the three-body repulsive barrier, see Appendix D for more detail. The contrast highlights the underlying multichannel nature in our observation in Fig. 7

C. Analysis in spin-position space

To gain a better physical understanding of the origin of the observations made in the previous section, it is instructive to consider explicitly the multichannel structure of the three-body problem. In the open-channel state $|aa, a\rangle$, every pair of particles interacts via the strongly resonant van der Waals interaction which induces the Efimov effect. Together with the suppression of two-body probability when $r < r_{\text{vdW}}$, this will drive the particles towards equilateral three-body configurations which minimize the likelihood of small nuclear distances. As mentioned in the previous section, these dynamics are recognized in the hyperspherical picture via the nonadiabatic potential $Q_{00}(R)$, which forms a strong repulsive barrier at small hyperradii [12,13]. In the multichannel case, the physical picture is complicated by the presence of a three-body closed channel $|bc, a\rangle$. In this state there appears an asymmetry in the strength of the two-particle interactions, given that two of the three pairs exist in the nonresonant channels $|ab\rangle$ and $|ac\rangle$. Hence the interaction with the third particle is much weaker than the interaction felt by two particles in the $|aa\rangle$ state, which is resonantly enhanced.

With these effects in mind we now turn our attention once more to the results presented in Fig. 7. As we decrease s_{res} ,

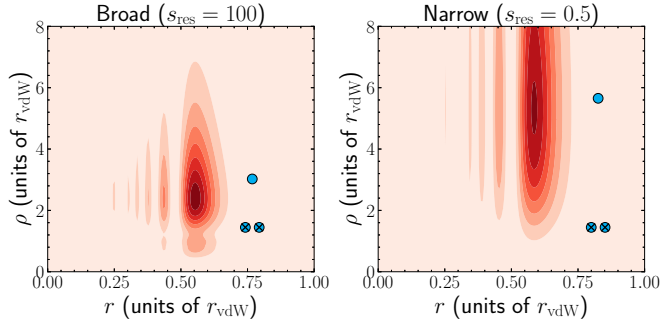


FIG. 8. Contour plots of three-body probability $P_{bc,a}(r, \rho) \sim r^2 \rho^2 |\langle r\rho; \underline{bc}, a | \Psi \rangle|^2$ in the plane of Jacobi coordinates r and ρ for a broad and narrow Feshbach resonance. Note that $\langle \underline{bc}, a | \Psi \rangle = \langle \underline{bc}, a | \bar{\Psi} \rangle$ since $\langle \underline{ab}, c | \bar{\Psi} \rangle$ and $\langle \underline{ac}, b | \bar{\Psi} \rangle$ vanish by neglecting nonresonant interactions [18]. The drawings show the changing structure of the Efimov state, where particles in the closed channel $|\underline{bc}\rangle$ are drawn with a cross.

the lifetime of the closed-channel state increases, scaling as $1/s_{\text{res}}$. The third atom then interacts with the pair $|\underline{bc}\rangle$ via a nonresonant van der Waals interaction, much weaker than the resonant interaction present for the broad resonance. This leads to a gradual decrease of the depth of the effective potential shown in Fig. 7, as the coupling to the closed channel $|\underline{bc}, a\rangle$ stretches the three-body state to more elongated configurations. To illustrate this behavior we computed the closed-channel component $\langle \underline{bc}, a | \bar{\Psi} \rangle$ of the three-body wave function, which can be directly obtained from Eq. (10) once $F_a(p)$ is computed. We then formulate the closed-channel three-body probability $P_{bc,a}$, plotted in Fig. 8. Here we clearly observe the stretching of the wave function that occurs near a narrow resonance, which is directed along the ρ coordinate quantifying the separation of the third particle. In the limit of a very narrow resonance, the third particle is free to drift towards separations far beyond r_{vdW} , consistent with a flat three-body potential. In contrast, the shape of the probability along the dimer separation r is relatively unaffected by the resonance strength, and in fact follows the structure of the two-body closed channel wave function as shown in Fig. 5. Figure 8 also shows that there is no repulsive barrier at small hyperradii in the closed channel state, which allows particles to approach to within the van der Waals range. The fact that a universal short-range repulsive barrier remains in $\langle \underline{aa}, a | \bar{\Psi} \rangle$ also for narrow resonances, as shown in Figs. 6 and 7, is due to the influence of the open-channel component, where a universal barrier due to $Q_{00}(R)$ always exists and is independent of resonance strength. This prevents coupling to the closed-channel state for small hyperradii, hence preserving the short-range suppression of the wave function, as clearly observed in Figs. 6 and 7.

As was discussed in Sec. III A, the relative weakness of nonresonant interactions is a commonly used assumption for the three-body problem. It is important to note that, while this assumption is valid for most systems, there are special cases where it is expected to be incorrect. For example, if the resonant closed channel state is taken as $|\underline{ab}\rangle$, i.e., just one particle changes its state, then both the open and closed channel three-body states have purely resonant interactions.

We expect this to alter the behavior of the three-body potential and indeed it was shown in Ref. [18] that for closed channels of this type the scaling of the three-body parameter with s_{res} is actually inverted. Additionally, our model is not expected to hold for strongly overlapping Feshbach resonances, where several channels have resonantly enhanced interactions simultaneously.

V. CONCLUSION AND OUTLOOK

In this work we analyzed the change in the Efimovian three-body potential as the Feshbach resonance strength is tuned from the broad to narrow resonance regime. For this purpose we developed a two-channel separable model that takes into account the full coupled-channels low-energy scattering wave function. Our numerical results show that, as the resonance strength is tuned away from the broad limit, the associated change in the three-body parameter a_- originates from a decrease of the three-body potential depth in the intermediate distance regime where $R > 2 r_{\text{vdW}}$. In contrast, the three-body repulsive barrier that is observed in single-channel models at $R \approx 2 r_{\text{vdW}}$ remains universally determined by the van der Waals length. We interpreted our observations to originate from the relative weakness of interactions between nonresonant spin-channels compared to the resonant interaction that exists in the open channel and drives the Efimov effect. Hence our results should apply generally to systems in which the Feshbach resonance is sufficiently isolated.

There are several possible opportunities for extensions of our approach. Our physical picture of the decreasing three-body attraction for narrow resonances rests on the assumption that the interaction between closed and open-channel particles is off-resonant, such that it may be neglected. Consequently, we expect that the presence of a resonant third-channel alters the behavior of the potential significantly, which could be accurately captured in a three-channel EST model. Another point of interest is the analysis of special closed-channel configurations of the type $|\underline{ab}\rangle$, where it is known that the value of $|a_-|$ decreases for a narrow resonance [18]. Such a system, however, is not easily analyzed with our model since the trimer wave function becomes more localized in the short-range where the effective three-body potential is not a useful construct.

ACKNOWLEDGMENTS

We thank Pascal Naidon and Thomas Secker for discussions. This research is financially supported by the Dutch Ministry of Economic Affairs and Climate Policy (EZK), as part of the Quantum Delta NL program and by the Netherlands Organisation for Scientific Research (NWO) under Grant No. 680-47-623.

APPENDIX A: TUNING OF FESHBACH RESONANCE PARAMETERS

In this Appendix we give some additional detail on the tuning of the parameters of our two-body multichannel interaction. A Feshbach resonance is typically parametrized by the

following relation [14]:

$$a(B) = a_{\text{bg}} \left(1 - \frac{\Delta B}{B - B_0} \right). \quad (\text{A1})$$

The background scattering length a_{bg} can be set directly by tuning the short-range parameter r_0 . The resonance width ΔB , is given as [14]

$$\Delta B \underset{k \rightarrow 0}{=} \frac{\pi}{a_{\text{bg}} k \delta \mu} |\langle \phi_{\text{res}} | V_{21} | \psi_\varepsilon \rangle|^2. \quad (\text{A2})$$

Here $|\phi_{\text{res}}\rangle$ is the unit normalized wave function of the resonant bound state, $|\psi_\varepsilon\rangle$ is the energy normalised scattering wave function in the open-channel, and $k = \sqrt{m\varepsilon/\hbar^2}$. We vary the parameters α and β until Eq. (A2) is satisfied for a given ΔB . Note that this mapping is not unique, but we numerically confirmed our results to be insensitive to different choices of α and β . The last parameter to fix is the bare resonance position B_{res} , which is shifted to B_0 by the presence of the spin-exchange interaction. In van der Waals potentials it is possible to approximate the relation between B_0 and B_{res} using the techniques of multichannel quantum defect theory (MQDT) [52–56]. This leads to the direct relation

$$B_0 = B_{\text{res}} + \left[\frac{r_{\text{bg}}(1 - r_{\text{bg}})}{1 + (1 - r_{\text{bg}})^2} \right] \Delta B, \quad (\text{A3})$$

where $r_{\text{bg}} = a_{\text{bg}}/\bar{a}$. With Eqs. (A1), (A2), and (A3) we can fix all the parameters of our model.

APPENDIX B: EST TWO-BODY TRANSITION MATRIX

In this Appendix we give explicit expressions for the momentum projection of the separable transition matrix in our multichannel EST separable potential. The function $\tau(z)$ follows from Eq. (7),

$$\begin{aligned} \tau^{-1}(z) = & \frac{m}{\hbar^2} \left[\frac{2\pi^2}{a} |g_1(0)|^2 \right. \\ & \left. + 4\pi \sum_{\sigma} \int_0^{\infty} dk \frac{k^2 \left(\frac{mz}{\hbar^2}\right) |g_{\sigma}(k)|^2}{\left(k^2 + \frac{m\varepsilon_{\sigma}}{\hbar^2}\right) \left(k^2 + \frac{m\varepsilon_{\sigma}}{\hbar^2} - \frac{mz}{\hbar^2}\right)} \right]. \end{aligned} \quad (\text{B1})$$

This form is inspired by Ref. [6] and uses the fact that the zero-energy on-shell transition matrix is related to the scattering length as $t_{1,1}(0, 0, 0) = \hbar^2 a / (2\pi^2 m)$. The form factors can be computed directly from Eq. (6), by inserting complete sets of position states. Our normalization gives $\langle \mathbf{r} | k, \sigma \rangle \sim \sin(kr)/(kr) |\sigma\rangle$ and we expand the scattering wave function into channel functions $u_{\sigma}(r)$ as

$$\langle \mathbf{r} | \psi \rangle \sim \sum_{\sigma} \frac{u_{\sigma}(r)}{r} |\sigma\rangle. \quad (\text{B2})$$

Then the form factors, normalized such that $g_1(0) = 1$, are given by

$$g_{\sigma}(k) = \frac{\sum_{\sigma'} \int_0^{\infty} dr \sin(kr) V_{\sigma, \sigma'}(r) u_{\sigma'}(r)}{k \sum_{\sigma'} \int_0^{\infty} dr r V_{1, \sigma'}(r) u_{\sigma'}(r)}, \quad (\text{B3})$$

where $V_{\sigma, \sigma'} = \langle \sigma | V | \sigma' \rangle$.

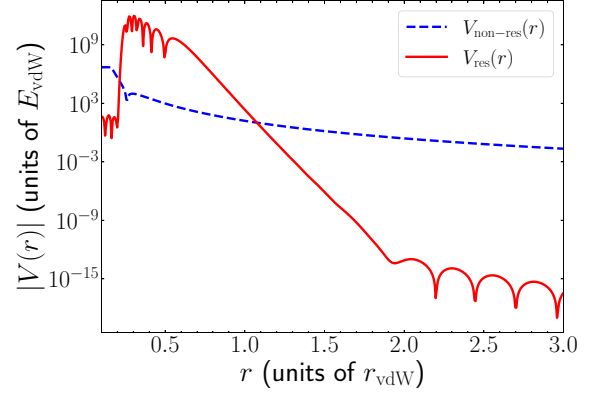


FIG. 9. Comparison of the absolute magnitude of the resonance enhanced interaction $V_{\text{res}}(r)$, with a nonresonant van der Waals interaction $V_{\text{non-res}}(r)$. Note that for $V_{\text{res}}(r)$ the diagonal elements of the nonlocal potential matrix are plotted. Energy given in units of $E_{\text{vdW}} = \hbar^2/(mr_{\text{vdW}}^2)$.

APPENDIX C: COMPARISON OF RESONANT TO NONRESONANT INTERACTIONS

The fixed spectating spin reduction of the multichannel STM equation, as discussed in Sec. III A, rests on the assumption that interactions in the nonresonant closed channels $|ab, c\rangle$ and $|ac, b\rangle$ are negligible compared to the resonance enhanced channel $|bc, a\rangle$. To illustrate numerically that this is a reasonable assumption, we parametrize the effective interaction in the $|bc\rangle$ channel by computing an EST separable potential V_{res} , associated with the resonant two-body bound state $|\varphi_{\text{res}}\rangle$. It is formulated as

$$V_{\text{res}} = V_{bc, bc} |\varphi_{\text{res}}\rangle \langle \varphi_{\text{res}} | V_{bc, bc} |\varphi_{\text{res}}\rangle^{-1} \langle \varphi_{\text{res}} | V_{bc, bc}. \quad (\text{C1})$$

In Fig. 9 we compare the magnitude of $\langle \mathbf{r} | V_{\text{res}} | \mathbf{r} \rangle$ to the van der Waals interaction without any resonant enhancement $V_{\text{non-res}}$. One clearly observes that the resonant enhancement augments the bare interaction by several orders of magnitude, which supports the assumption made in Sec. III A.

APPENDIX D: COMPARISON WITH NUCLEAR INTERACTIONS

In Sec. IV C we argue that our observations in the multichannel model arise due to a distinct interplay between the different possible spin-states on the three-body level. It is

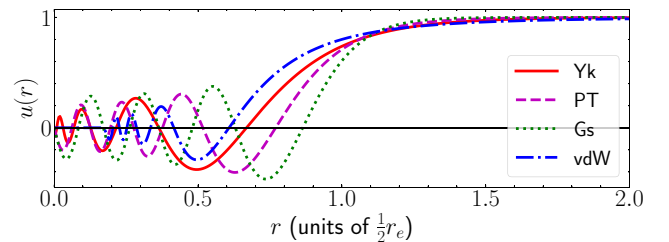


FIG. 10. Two-body radial wave functions at the appearance of the eighth potential resonance of the three nuclear interactions in Eq. (D1) and the van der Waals (vdW) interaction in Eq. (2). All distances are expressed in the associated effective range scale $r_e/2$.

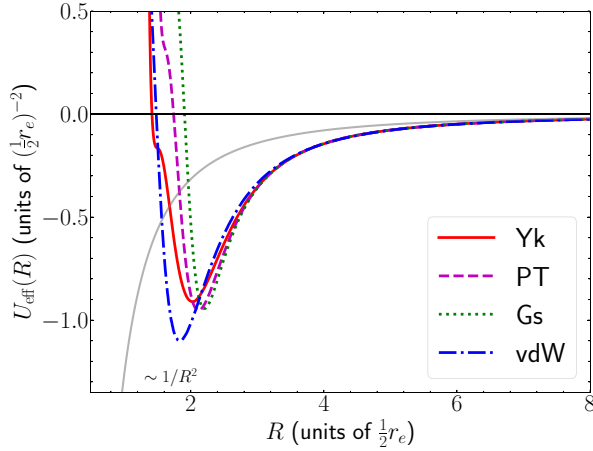


FIG. 11. Plot of the effective three-body potential as a function of the hyperradius, in units of the effective range. Colored lines show the effective potential for different shapes of the two-body interaction, tuned to a depth of eight dimer states. The gray line shows the asymptotic $\sim 1/R^2$ Efimov attraction as follows from the zero-range theory.

known, however, that the value of $|a_-|$ can also increase with different kinds of asymptotic three-body interactions, without any need for additional spin-channels. In this Appendix we contrast the changing three-body potential in systems of this type with our previous multichannel results to show that the underlying mechanisms are indeed fundamentally different. Specifically, we will consider single-channel EST models based on two-body interactions that decay exponentially in the long range, common in nuclear physics. For this class of interactions the short-range two-body suppression looks rather different from the van der Waals potential, where “short-range” is now interpreted as $r < r_e/2$, with r_e the effective range constant. To illustrate the differences we plot in Fig. 10 the two-body wave function at unitarity for the following set

of nuclear potentials:

$$\begin{aligned} V_{\text{PT}} &\sim -\eta \cosh^{-2}(r), \\ V_{\text{Yk}} &\sim -\frac{\eta}{r} \exp(-r), \\ V_{\text{Gs}} &\sim -\eta \exp(-r^2), \end{aligned} \quad (\text{D1})$$

which, respectively, are the usual Pöschl-Teller (PT), Yukawa (Yk), and Gaussian (Gs) potentials [12,26]. The strength parameter η is used to tune the potential towards resonance. Similar to the case of van der Waals interactions, the short-range suppression in the two-body wave function leads to the formation of a three-body repulsive barrier and hence a universal value for the three-body parameter in the limit of broad Feshbach resonances. As was shown in Ref. [26], this universal value matches the three-body parameter that one obtains when using a simple step function as input into the EST model, which is zero for $r < r_e/2$ and unity everywhere else. Indeed for an infinite number of two-body bound states the PT, Yk, and Gs wave functions in Fig. 10, will all approach step functions [26]. This is not the case for the interaction in Eq. (2) whose infinitely deep limit is obtained by taking $r_0 \rightarrow 0$, yielding a pure (but ill-behaved) van der Waals potential. Interestingly for this work is the fact that the three-body parameter $|a_-|$ obtained from the step-function limit in a single-channel model is $\sim 19\%$ larger than the value obtained from the van der Waals interaction [26]. In our multichannel model we similarly observe an increased value of $|a_-|$ when s_{res} is decreased away from the broad resonance limit. Evidently, however, the associated change in the two-body wave function is very different, as becomes clear when comparing Figs. 5 and 10. Whereas in the multichannel model the open-channel component that underlies the Efimov state was unchanged, for the interactions in this section there is a clear change in the short-range suppression in the open channel. As shown in Fig. 11, this subsequently leads to a shift in the location of the three-body barrier, which is absent in the multichannel model as explained in Sec. IV C.

-
- [1] V. Efimov, *Phys. Lett. B* **33**, 563 (1970).
 - [2] V. Efimov, *Sov. J. Nucl. Phys.* **12**, 589 (1971).
 - [3] B. D. Esry, C. H. Greene, and J. P. Burke, *Phys. Rev. Lett.* **83**, 1751 (1999).
 - [4] T. Kraemer, M. Mark, P. Waldburger, J. G. Danzl, C. Chin, B. Engeser, A. D. Lange, K. Pilch, A. Jaakkola, H.-C. Nägerl, and R. Grimm, *Nature (London)* **440**, 315 (2006).
 - [5] E. Braaten and H.-W. Hammer, *Phys. Rep.* **428**, 259 (2006).
 - [6] P. Naidon and S. Endo, *Rep. Prog. Phys.* **80**, 056001 (2017).
 - [7] M. Berninger, A. Zenesini, B. Huang, W. Harm, H.-C. Nägerl, F. Ferlaino, R. Grimm, P. S. Julienne, and J. M. Hutson, *Phys. Rev. Lett.* **107**, 120401 (2011).
 - [8] N. Gross, Z. Shotan, O. Machtey, S. Kokkelmans, and L. Khaykovich, *C. R. Phys.* **12**, 4 (2011).
 - [9] P. Dyke, S. E. Pollack, and R. G. Hulet, *Phys. Rev. A* **88**, 023625 (2013).
 - [10] R. J. Wild, P. Makotyn, J. M. Pino, E. A. Cornell, and D. S. Jin, *Phys. Rev. Lett.* **108**, 145305 (2012).
 - [11] R. Chapurin, X. Xie, M. J. Van de Graaff, J. S. Popowski, J. P. D’Incao, P. S. Julienne, J. Ye, and E. A. Cornell, *Phys. Rev. Lett.* **123**, 233402 (2019).
 - [12] J. Wang, J. P. D’Incao, B. D. Esry, and C. H. Greene, *Phys. Rev. Lett.* **108**, 263001 (2012).
 - [13] P. Naidon, S. Endo, and M. Ueda, *Phys. Rev. A* **90**, 022106 (2014).
 - [14] C. Chin, R. Grimm, P. Julienne, and E. Tiesinga, *Rev. Mod. Phys.* **82**, 1225 (2010).
 - [15] G. F. Gribakin and V. V. Flambaum, *Phys. Rev. A* **48**, 546 (1993).
 - [16] D. S. Petrov, *Phys. Rev. Lett.* **93**, 143201 (2004).
 - [17] Y. Nishida, *Phys. Rev. Lett.* **109**, 240401 (2012).
 - [18] T. Secker, D. J. M. Ahmed-Braun, P. M. A. Mestrom, and S. J. J. M. F. Kokkelmans, *Phys. Rev. A* **103**, 052805 (2021).
 - [19] F. H. Mies, E. Tiesinga, and P. S. Julienne, *Phys. Rev. A* **61**, 022721 (2000).
 - [20] N. Nygaard, B. I. Schneider, and P. S. Julienne, *Phys. Rev. A* **73**, 042705 (2006).

- [21] Y. Wang and P. Julienne, *Nat. Phys.* **10**, 768 (2014).
- [22] The advantage of using the r^{-10} core instead of the more traditional r^{-12} shape is the fact that the associated zero-energy scattering problem allows for an exact solution in terms of hyperconfluent geometric functions. Thus the length scale r_0 can be analytically related to the scattering length, making it straightforward to fix a_{bg} . This interaction was characterized by Pade, cited in the next reference.
- [23] J. Pade, *Eur. Phys. J. D* **44**, 345 (2007).
- [24] This value was chosen for approximate correspondence with the coupling in the realistic multichannel ^{39}K potential as formulated in Ref. [43]. As expected, our results are largely insensitive to changes in r_W since they are compensated by a corresponding change in β , with the caveat that r_W should remain significantly smaller than r_{vdW} .
- [25] T. Secker, J.-L. Li, P. M. A. Mestrom, and S. J. J. M. F. Kokkelmans, *Phys. Rev. A* **103**, 022825 (2021).
- [26] P. Naidon, S. Endo, and M. Ueda, *Phys. Rev. Lett.* **112**, 105301 (2014).
- [27] D. Ernst, C. Shakin, and R. Thaler, *Phys. Rev. C* **8**, 46 (1973).
- [28] J. Taylor, *Scattering Theory: The Quantum Theory of Nonrelativistic Collisions*, 1st ed. (Dover, New York, 2006).
- [29] K. Willner, O. Dulieu, and F. Masnou-Seeuws, *J. Chem. Phys.* **120**, 548 (2004).
- [30] T. Secker, J.-L. Li, P. M. A. Mestrom, and S. J. J. M. F. Kokkelmans, *Phys. Rev. A* **103**, 032817 (2021).
- [31] T. Karman, L. M. C. Janssen, R. Sprenkels, and G. C. Groenenboom, *J. Chem. Phys.* **141**, 064102 (2014).
- [32] L. Faddeev, *Sov. Phys. JETP* **12**, 1014 (1961).
- [33] W. Glöckle, *The Quantum Mechanical Few-Body Problem*, Texts and Monographs in Physics (Springer, Berlin, 1983).
- [34] A. O. Gogolin, C. Mora, and R. Egger, *Phys. Rev. Lett.* **100**, 140404 (2008).
- [35] P. Massignan and H. T. C. Stoof, *Phys. Rev. A* **78**, 030701(R) (2008).
- [36] R. Schmidt, R. Rath, and W. Zwerger, *Eur. Phys. J. B* **85**, 386 (2012).
- [37] C. Langmack, R. Schmidt, and W. Zwerger, *Phys. Rev. A* **97**, 033623 (2018).
- [38] J.-L. Li, T. Secker, P. M. A. Mestrom, and S. J. J. M. F. Kokkelmans, *Phys. Rev. Res.* **4**, 023103 (2022).
- [39] J. Macek, *J. Phys. B: At. Mol. Phys.* **1**, 831 (1968).
- [40] J. Macek, *Z. Phys. B* **3**, 31 (1986).
- [41] E. Nielsen, D. Fedorov, A. Jensen, and E. Garrido, *Phys. Rep.* **347**, 373 (2001).
- [42] E. Braaten, H.-W. Hammer, and M. Kusunoki, *Phys. Rev. A* **67**, 022505 (2003).
- [43] S. Falke, H. Knöckel, J. Friebe, M. Riedmann, E. Tiemann, and C. Lisdat, *Phys. Rev. A* **78**, 012503 (2008).
- [44] N. R. Claussen, S. J. J. M. F. Kokkelmans, S. T. Thompson, E. A. Donley, E. Hodby, and C. E. Wieman, *Phys. Rev. A* **67**, 060701(R) (2003).
- [45] A. Derevianko, W. R. Johnson, M. S. Safronova, and J. F. Babb, *Phys. Rev. Lett.* **82**, 3589 (1999).
- [46] M. Berninger, A. Zenesini, B. Huang, W. Harm, H.-C. Nägerl, F. Ferlaino, R. Grimm, P. S. Julienne, and J. M. Hutson, *Phys. Rev. A* **87**, 032517 (2013).
- [47] B. Gao, *Phys. Rev. A* **84**, 022706 (2011).
- [48] F. Werner and Y. Castin, *Phys. Rev. A* **86**, 013626 (2012).
- [49] V. V. Flambaum, G. F. Gribakin, and C. Harabati, *Phys. Rev. A* **59**, 1998 (1999).
- [50] S. Roy, M. Landini, A. Trenkwalder, G. Semeghini, G. Spagnolli, A. Simoni, M. Fattori, M. Inguscio, and G. Modugno, *Phys. Rev. Lett.* **111**, 053202 (2013).
- [51] T. Köhler, K. Góral, and P. S. Julienne, *Rev. Mod. Phys.* **78**, 1311 (2006).
- [52] C. H. Greene, A. R. P. Rau, and U. Fano, *Phys. Rev. A* **26**, 2441 (1982).
- [53] F. H. Mies, *J. Chem. Phys.* **80**, 2514 (1984).
- [54] F. H. Mies and P. S. Julienne, *J. Chem. Phys.* **80**, 2526 (1984).
- [55] K. Jachymski and P. S. Julienne, *Phys. Rev. A* **88**, 052701 (2013).
- [56] P. Naidon and L. Pricoupenko, *Phys. Rev. A* **100**, 042710 (2019).

Correction: A typographical error introduced during the production process involving the characters inside angular brackets in Eqs. (10) and (14) and in various locations in text has been fixed.